

# Nanoscale

Accepted Manuscript



This is an *Accepted Manuscript*, which has been through the Royal Society of Chemistry peer review process and has been accepted for publication.

*Accepted Manuscripts* are published online shortly after acceptance, before technical editing, formatting and proof reading. Using this free service, authors can make their results available to the community, in citable form, before we publish the edited article. We will replace this *Accepted Manuscript* with the edited and formatted *Advance Article* as soon as it is available.

You can find more information about *Accepted Manuscripts* in the [Information for Authors](#).

Please note that technical editing may introduce minor changes to the text and/or graphics, which may alter content. The journal's standard [Terms & Conditions](#) and the [Ethical guidelines](#) still apply. In no event shall the Royal Society of Chemistry be held responsible for any errors or omissions in this *Accepted Manuscript* or any consequences arising from the use of any information it contains.

Cite this: DOI: 10.1039/c0xx00000x

www.rsc.org/xxxxxx

ARTICLE TYPE

# Protein Denaturation at Single-molecule Level: The Effect of Nonpolar Environments and Its Implications to the Unfolding Mechanism by Proteases

Bo Cheng,<sup>a</sup> Shaogui Wu,<sup>b</sup> Shixin Liu,<sup>c</sup> Piere Rodriguez,<sup>c</sup> Jin Yu,<sup>\*,b</sup> and Shuxun Cui<sup>\*,a</sup><sup>5</sup> Received (in XXX, XXX) Xth XXXXXXXXXX 20XX, Accepted Xth XXXXXXXXXX 20XX

DOI: 10.1039/b000000x

Most proteins are typically folded into predetermined three-dimensional structures in the aqueous cellular environment. However, proteins can be exposed to a nonpolar environment under certain conditions, such as inside the central cavity of chaperones and unfoldases during protein degradation. It remains unclear how folded proteins behave when moved from an aqueous solvent to a nonpolar one. Here, we employed single-molecule atomic force microscopy and molecular dynamics (MD) simulations to investigate the structural and mechanical variations of a polyprotein, I27<sub>8</sub>, during a change from polar to nonpolar environment. We found that the polyprotein was unfolded into an unstructured polypeptide spontaneously when pulled into nonpolar solvents. This finding was corroborated by MD simulations where I27 was dragged from water into a nonpolar solvent, revealing details of the unfolding process at the water/nonpolar solvent interface. These results highlight the importance of water in maintaining folding stability, and provide insights into the response of folded proteins to local hydrophobic environments.

## 1. Introduction

In the physiological environment, proteins are typically folded into well-defined three-dimensional structures that determine their activities *in vivo*. As the reverse process of folding, protein unfolding is also important in a number of biological processes, such as translocation across membranes<sup>1</sup> and degradation by ATP-fueled proteases.<sup>2</sup> Denaturants (such as guanidinium chloride) or highly polar organic solvents (such as dimethyl sulfoxide, DMSO) induce complete unfolding of proteins *in vitro*.<sup>3</sup> Nevertheless, a different unfolding mechanism should be exploited *in vivo* by chaperones and unfoldases, which are thought to perform their tasks by exposing proteins to hydrophobic environments.

Although water plays an important role on the protein folding, it is difficult to discern the effects of water molecules in aqueous environment.<sup>4, 5</sup> To this end, one should observe the behaviour of a protein in a non-aqueous environment, especially a nonpolar solvent. Since proteins are insoluble in all nonpolar

solvents, the structural changes upon environmental alteration can be hardly observed by traditional ensemble measurements. Here, atomic force microscope (AFM)-based single-molecule force spectroscopy (SMFS)<sup>6-31</sup> provides a way to overcome this obstacle by making it possible to pull into solvents in which they are not soluble. More importantly, single-molecule pulling experiments can mimic the process of environment change as it may occur under the physiological action of unfoldases: single proteins can be pulled through a polar/nonpolar interface while their structural changes are monitored simultaneously.

Here, we investigated the impact of the environmental change on the mechanical stability of a polyprotein, polyI27, by two complementary methods: AFM-based SMFS and molecular dynamics (MD) simulations.<sup>32, 33</sup> We prepared a polyI27 sample at a surface and exchanged the aqueous buffer with a nonpolar solvent (Scheme S1 in ESI), such as octane and octylbenzene. SMFS results indicate that polyI27 exists in its native tandem globule structure in an aqueous buffer, whereas in nonpolar solvents, polyI27 is denatured into unstructured polypeptides. This experimental result was supported by MD simulations, in which the I27 globule was observed to unfold completely at the interface when it was pulled from water to a nonpolar solvent. The results from both experimental and simulation studies not only provide direct evidence on the importance of water to the protein structure, but also cast new light on the mechanism of protein unfolding by polar/nonpolar boundaries.

## 2. Experimental section

### 2.1 Materials and Sample preparation.

The I27<sub>8</sub> (Athena Environmental Sciences, Inc., MD) is a 94 kDa synthetic polyprotein composed of eight repeats of the I27 domain of human titin protein.<sup>20</sup> Deionized (DI) water (>15MΩ·cm) was used in all the experiments. All other chemical reagents were purchased from Sigma and were analytically pure, unless mentioned otherwise. For the sample preparation, the I27<sub>8</sub> was diluted with PBS buffer (pH=7.4) to a final concentration of 100 μg/ml. I27<sub>8</sub> was allowed to adsorb physically onto a freshly evaporated gold surface for 12 h, followed by rinsing with PBS buffer to remove the loosely adsorbed molecules.<sup>6</sup> After dried by

air flow, the sample was ready to use in force measurements. Polylysine (MW $\geq$ 300,000, Sigma Inc.) was also diluted with PBS buffer to a final concentration of 100  $\mu$ g/ml. The preparation of polylysine sample for the force measurements was similar to that of I27<sub>8</sub>.

## 2.2 Force measurements.

All force experiments were carried on a commercial AFM (MFP-3D, Asylum Research, CA). Prior to the measurements, a drop of the PBS buffer solution (or nonpolar solvent) was injected between the Si<sub>3</sub>N<sub>4</sub> AFM cantilever (MSCT model, Bruker Corp., CA) and the sample. Then during the AFM manipulation, the data were recorded at the same time and converted to force-extension curves (in brief, F-E curves) subsequently. The spring constant of each AFM cantilever was calibrated by the thermo-excitation method. Values ranged between 20 to 50 pN/nm. The stretching velocity was 2.0  $\mu$ m/s unless mentioned otherwise. The experimental details of SMFS can be found elsewhere.<sup>8, 18, 34, 35</sup> To compare the different F-E curves, these curves were normalized by the extension that correspond to the same force value (e.g. 200 pN).

## 2.3 MD Simulation on Pulling Protein.

The titin crystal structure (PDB code: 1TIT) reported by Im-prota *et al.*<sup>36</sup> is used as the initial configuration. TIP3P water model is used for the explicit solvent.<sup>37</sup> The simulation system consists of  $\sim$ 77000 atoms (394 $\text{\AA}$   $\times$  44  $\text{\AA}$   $\times$  44  $\text{\AA}$ ), including 5693 water molecules, 2268 octane molecules, and the protein molecule. Additionally 14 sodium and 8 chloride ions are added to

make the system electrically neutral (the aqueous phase is a  $\sim$ 0.075 M salt solution). Each simulation is performed in the NPT ensemble (1 atm and 310 K) using the NAMD<sup>38</sup> simulation package and the CHARMM27 force field,<sup>39</sup> with an integration time step of 1 fs and periodic boundary conditions; van der Waals (vdW) energies are calculated using a smooth cutoff (10-12 $\text{\AA}$ ); and the particle-mesh Ewald method is employed for full electrostatics.<sup>40</sup> After energy minimization, the simulation system is equilibrated for 1 ns. Then a harmonic spring (with a force constant of 5 nN/nm) is attached at the C $\alpha$  atom at the terminal residue LEU89 (C terminal). The protein is pulled vertically from water to octane at a constant speed of 2 $\text{\AA}$ /ns, perpendicular to the interface between water and octane. During the pulling process, the center of mass of the octane phase is constrained to avoid shifting of the octane layer.

## 3. Results and Discussion

### 3.1 Structures of PolyI27 in Water and Nonpolar Solvents.

We first monitored the unfolding behaviour of I27<sub>8</sub> in the PBS buffer. The typical “saw-tooth” F-E curve was obtained (Fig. 1A), which reflected the consecutive unfolding of individual domains of the polyprotein. The characteristic “saw-tooth” pattern can be explained as stepwise increase in the contour length of the I27<sub>8</sub> chain, whose elastic properties can be generally described by the worm-like chain (WLC) model<sup>34, 41-43</sup> (Fig. 1A, red dotted lines). The WLC fitting curve reveals a space of  $\Delta L=28$  nm between two adjacent peaks, in good agreement with the contour length of an I27 domain.<sup>6, 44</sup> These results indicate that I27<sub>8</sub> is in its native folded structure in the PBS buffer.

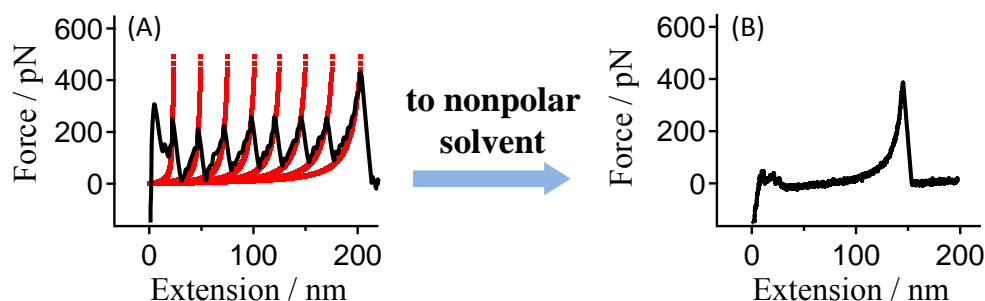


**Fig. 1.** Typical F-E curves of I27<sub>8</sub> in PBS buffer and octylbenzene. We use SMFS method to investigate the mechanical behavior of I27<sub>8</sub> molecule in different liquid environments. A) The obtained F-E curve of I27<sub>8</sub> in PBS buffer is shown in black line, and the WLC model fitting curves are shown in red dotted lines (persistence length ( $l_p$ ) = 0.4 nm). B) The typical F-E curve of I27<sub>8</sub> obtained in octylbenzene.

Next, we exchanged the PBS buffer to a nonpolar organic solvent, octylbenzene, which is a poor solvent for proteins, and repeated the force-extension measurements with the I27<sub>8</sub> sample. In these conditions, the characteristic “sawtooth” curves were no longer observed. Instead, only a single peak was detected in each F-E curve (Fig. 1B). The force rises monotonically with extension until the molecule bridge between the AFM tip and substrate is broken. The F-E curves from different single molecules can be superposed with each other after normalization (Fig. 2), indicat-

ing that the F-E curves present the same mechanical properties.<sup>5, 45</sup> We have carried out similar force measurements in nonpolar solvent with varied stretching velocity (0.03–4  $\mu$ m/s), and observed no velocity dependence (see ESI for details). In addition, we carried out similar experiments by returning the environment from the nonpolar solvent to a PBS buffer. The reappearance of the “sawtooth” pattern in the F-E curve (see ESI for details) indicates that the solvent induced denaturation is completely reversible.

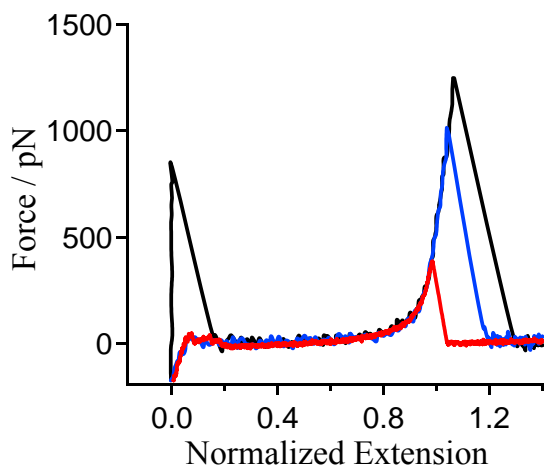


Fig. 2. The comparison of normalized F-E curves obtained from an I27<sub>8</sub> sample in octylbenzene.

5

One possible reason for the surprising result in octylbenzene (Fig. 2) is that the aromatic group in octylbenzene may show high affinity to the aromatic residues in the protein, such as phenylalanine. To exclude the aromatic stacking effect from octylbenzene, another nonpolar organic solvent that lacks the aromatic group, octane, is used in the F-E measurements. Fig. 3 compares the normalized F-E curves obtained in the two different nonpolar solvents. We observed no evident difference between the results obtained in octylbenzene and octane. Thus, the observed result in octylbenzene is not caused by aromatic stacking effect, but indeed by the environment change from aqueous buffer to a nonpolar solvent.

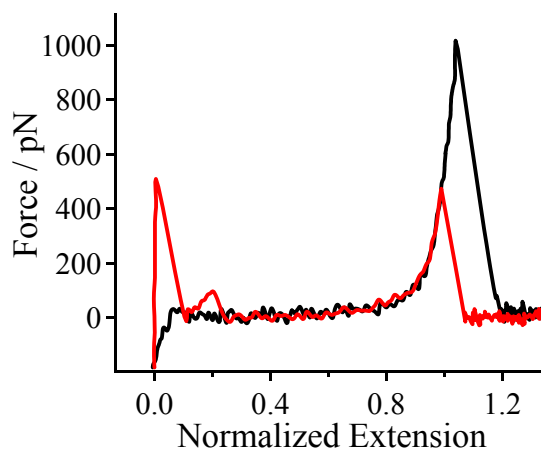


Fig. 3. The comparison of normalized F-E curves of I27<sub>8</sub> obtained in octylbenzene (black line) and octane (red line).

Note that the "single peak" event (Fig. 1B) occurs at a distance (~130 nm) much larger than the contour length of one I27 globule (~28 nm), implying that we observed a polypeptide that included all the unfolded I27 domains. To strengthen this conclu-

25

65

sion, we compared the experimental F-E curves with a theoretical predicted stretching behaviour of an unfolded polypeptide based on a QM-WLC model.<sup>46, 47</sup> In the QM-WLC model (Eq 1), the single-molecule elasticity of a peptide chain obtained from an advanced *ab initio* quantum mechanical (QM) calculation<sup>46</sup> is integrated into the WLC model:

$$F \frac{l_p}{k_B T} = \frac{R/L_0}{L[F]/L_0} + \frac{1}{4(1-(R/L_0))/(L[F]/L_0)^2} - \frac{1}{4} \quad (1)$$

where  $F$  is the stretching force,  $L[F]$  is the contour length of the macromolecule upon stretching with  $F$ ,  $L_0$  is the contour length at zero force,  $R/L_0$  is the normalized extension of a polymer chain,  $l_p$  is the persistence length,  $k_B$  is the Boltzmann constant, and  $T$  is the absolute temperature.

The chain elasticity is nonlinear, which can be expressed in a polynomial expansion (Eq 2) to provide the basis for a numerical fit of the measured F-E curves:

$$F = \sum_{n=1}^2 \gamma_n \left( \frac{L[F]}{L_0} - 1 \right)^n \quad \gamma_1 = 27.4 \text{ nN}, \gamma_2 = 109.8 \text{ nN} \quad (2)$$

where  $\gamma_1$  is the linear elastic modulus, and  $\gamma_2$  is a non-linear correction, which is important in the high force region.<sup>46</sup>

As shown in Fig. 4, the experimental F-E curve can be fitted well by the QM-WLC model when  $l_p = 0.38$  nm (see ESI for details), which is exactly the predicted length of one residue for a polypeptide.<sup>48</sup> The excellent consistency between experimental and theoretical F-E curves indicates that the I27<sub>8</sub> molecule is unfolded into an unstructured polypeptide when the aqueous buffer is changed to a nonpolar solvent.

45

50

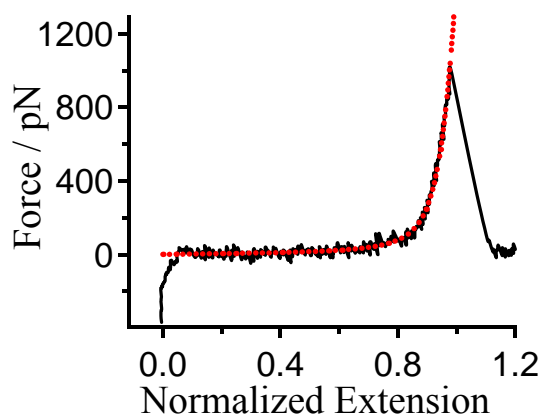
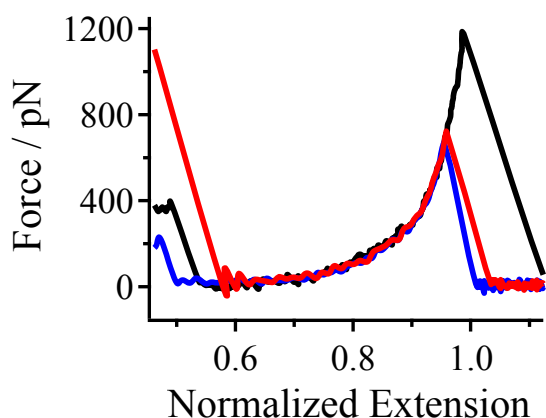


Fig. 4. The comparison of normalized F-E curves of I27<sub>8</sub> obtained in octylbenzene (black line) and the QM-WLC fitting curve with  $l_p = 0.38$  nm (red dotted line).

It is known that proteins denature into an unstructured polypeptide in the solutions with high concentration of denaturant, such as 6M guanidine•HCl (GdnHCl) solution.<sup>3</sup> We carried out the force measurements of I27<sub>8</sub> in a 6M GdnHCl solution, and again found only one peak in each F-E curve (Fig. 5), similar to the F-E curves of I27<sub>8</sub> in a nonpolar solvent (Fig. 1B, 2 and 3). These results further support that the F-E curves of I27<sub>8</sub> observed in nonpolar solvents correspond to a denatured state of a polypeptide.

60

65



**Fig. 5.** The comparison of normalized F-E curves of I27<sub>8</sub> obtained in a 6M GdnHCl solution.

Although the above results demonstrate that the I27 domains are in the denatured status (Fig. 1B, 2 and 3), a direct comparison with the experimental F-E curve of an unstructured polypeptide will be more convincing. Fig. 6 shows the normalized F-E curves of polylysine and I27<sub>8</sub> both obtained in a nonpolar solvent. Because the polylysine chain definitely has no specific 3D structure (Fig. S1 and S2 in ESI), the perfect superposition of the two F-E curves in Fig. 6 provides direct evidence that I27<sub>8</sub> chain is denatured into the unfolded state when the aqueous buffer is changed to a nonpolar solvent.

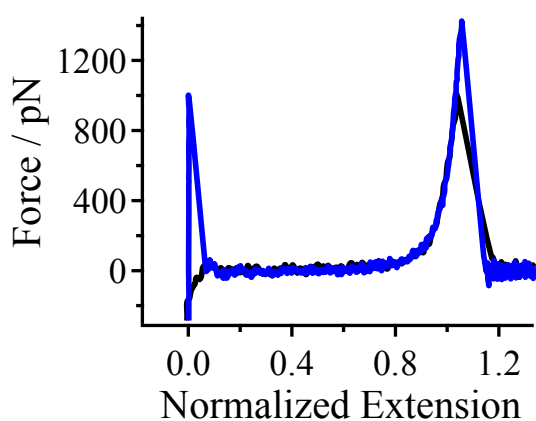


**Fig. 6.** The comparison of F-E curves of I27<sub>8</sub> (black line) and polylysine (blue line) that both obtained in octylbenzene.

### 3.2 Two Possible Scenarios for the Denaturation of Polyproteins.

The denaturation of polyproteins observed in nonpolar solvents can be associated with two possible scenarios. The first scenario is that the polyprotein is denatured when immersed in a nonpolar solvent, *i.e.*, the protein is denatured before pulling. The second scenario is associated with the interface between the aqueous solution and nonpolar solvent. It has been reported that water can be adsorbed onto the sample surfaces (such as gold and

glass) even in a dry environment, and form nano-films on the surfaces.<sup>49</sup> The adsorbed water film is expected to be retained when a water immiscible organic solvent (such as octylbenzene) is layered onto the sample surface. Moreover, it has been shown that the hydration layer of proteins will remain intact even when proteins are immersed in a nonpolar solvent.<sup>50</sup> In this scenario, the protein is actually dragged from water to the nonpolar solvent in the AFM measurements, *i.e.*, the protein is denatured during pulling across the interface.

To find out the protein unfolding mechanism, we carried out MD simulations for each of the two scenarios.

### 3.3 MD Simulations for the Two Scenarios.

For the first scenario, the I27 protein is placed directly into octane and then equilibrate the system. Unfolding has not been observed in simulation (see movie in ESI). Interestingly, in pioneering studies by Klibanov et al.,<sup>51</sup> they also observed that enzymes still had catalytic activities in nonpolar solvents. However, in a previous study, we found that double-stranded DNA (dsDNA) will be denatured by the repulsion force between the negative charges when it is placed in the nonpolar solvent.<sup>4,5</sup> For a typical protein, the charge density of the backbone is much lower than that of DNA. Moreover, both positive and negative charges exist in the backbone of a protein. Thus, the repulsion force in protein would be much lower than that in dsDNA, which is not high enough to unfold the protein.

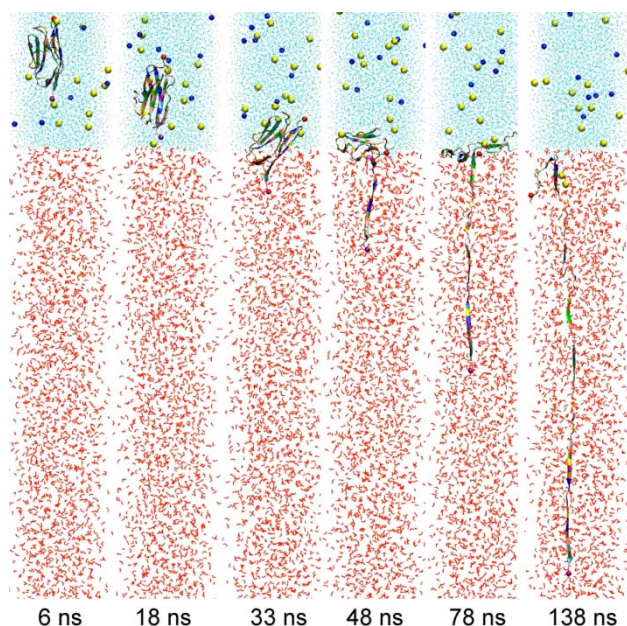


**Fig. 7.** MD simulation of pulling titin from water into octane. The protein is shown in cartoon presentation and colored according to residue name; water is colored in cyan and octane is shown in red; chloride and sodium ions are colored in blue and yellow, respectively; the C<sub>α</sub> atoms in the leading C terminal and the lagging N terminal are shown in purple and red, respectively. A harmonic spring (with a force constant of 5 nN/nm) was attached to the C<sub>α</sub> atom of the C terminal and was pulled down at a constant speed of 2 Å/ns. In the simulation, there are 6 snapshots taken at time  $t = 6, 18, 33, 48, 78$  and 138 ns, with protein unfolding starting at about  $t = 33$  ns as it is pulled into octane.

Although the protein is not unfolded in the simulation, it is observed that the root-mean-square-deviation (RMSD) of protein

is larger in octane than that in water, suggesting that the octane environment induces a partial conformation change of the protein (see ESI for details). This result is reasonable, since no hydrophobic force exists in octane, which is an important factor that stabilizes the original protein structure.<sup>52</sup>

For the second scenario, one titin I27 domain is dragged from aqueous solution to a nonpolar solvent, octane (see movie in ESI), which clearly demonstrates unfolding of the protein as it crosses the interface. The simulation lasts about 150 ns, pulling the protein at a speed of 2 Å/ns. Initially, the protein is moved smoothly through water, keeping its globular form. The protein conformation can be seen in molecular graphics in Fig. 7. The smooth process of pulling through water is revealed from the relatively stable and small forces needed during the process (Fig. 8A, the circled region in the diagram).

At about 20 ns, the leading terminal of the protein arrives at the water/octane interface and the pulling force begins to increase, indicating a resistance of the protein to the poor solvent environment. A possible reason for the resistance is that the outmost layer of a globule protein is hydrophilic and will be hydrated in water. It is unfavorable for the hydration shell to enter into the oil phase. At this moment, the protein starts to deform while being tilted to the oil-water interface. The deformation and tilting seem to expose an increasing contact area of the protein to the interface, leading to an increased resistance. During the period from 20 ns to 33 ns, the pulling force increases significantly from ~100 pN to ~1000 pN. As the full globular part of the protein aligns right

across the water/oil interface, the pulling force reaches a maximum. Then the protein starts to unfold, and the pulling force decreases sharply right after. This can be clearly observed in Fig. 7 (at 33 and 48 ns) and Fig. 8A, respectively.

During pulling, the two terminal C<sub>α</sub> atoms keep a constant distance before 33 ns (Fig. 8B and C). After that, as the leading terminal is continually dragged downward, the lagging terminal stays further behind. The distance between them increases correspondingly, indicating the unfolding of the protein. The change of the radius of gyration (R<sub>gyr</sub>) of the protein shows the same tendency (Fig. 8D). The unfolding continues with the pulling until the protein is fully dragged into the octane phase with a completely unfolded structure (Fig. 7 at 138 ns). The pulling force begins to decrease after ~135 ns (Fig. 8A). Further large conformation changes are not observed. Since the viscosity of octane is smaller (~5×10<sup>-4</sup> Pa·s at room temperature) than that of water (~9×10<sup>-4</sup> Pa·s), the frictional effect cannot explain the protein unfolding as being dragged into octane.

Due to limited computation time, the MD simulation pulling titin from water to octane is conducted much faster (~10<sup>5</sup> times faster) than that happens in SMFS experiments. Nevertheless, we clearly observe unfolding of the protein during the pulling simulation.

The two simulations together confirm that the second scenario (*i.e.*, denature during pulling across the interface) should be the case in the AFM-Pulling measurements.

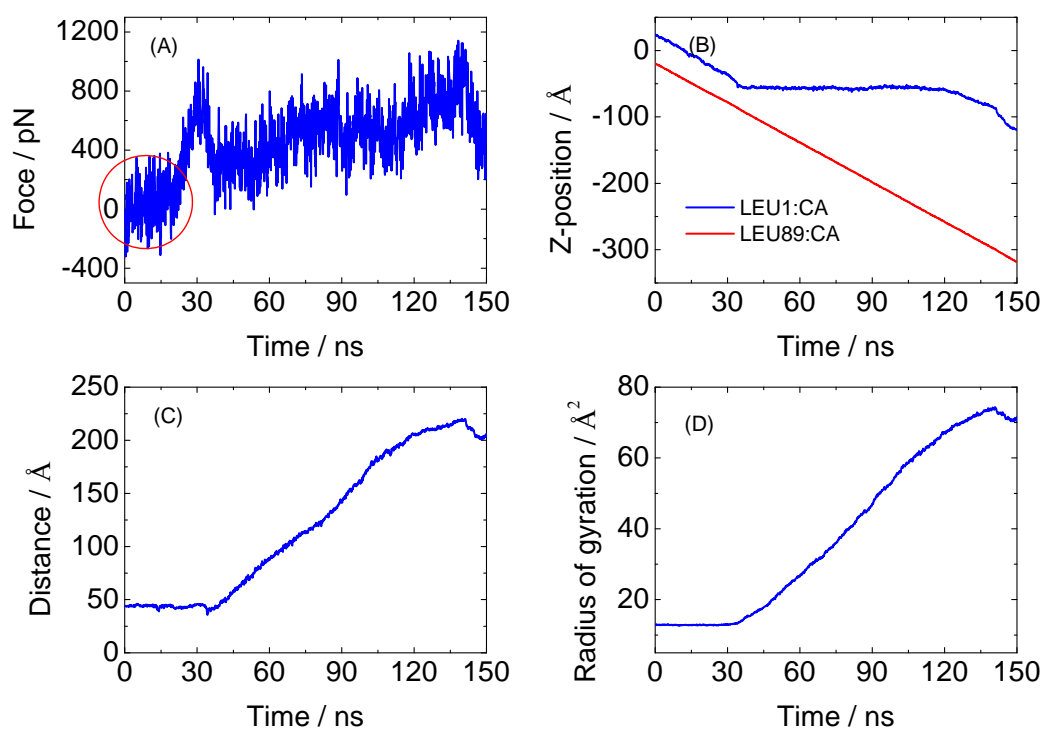


**Fig. 8.** Measurements from the MD simulation pulling titin from water to octane at a constant speed of 2 Å/ns. (A) The force applied to the terminal C<sub>α</sub> atom (seen as a purple vdW sphere in Fig. 7) vs simulation time. (B) The positions of the two terminal C<sub>α</sub> atoms of the protein along the pulling direction (z-axis) vs simulation time, the red line representing the leading C<sub>α</sub> atom being pulled, and the blue line for the lagging one. (C) The distance between two terminal C<sub>α</sub> atoms vs simulation time. (D) The radius of gyration (R<sub>gyr</sub>) vs simulation time. R<sub>gyr</sub> is determined using all the C<sub>α</sub> atoms in the protein as  $r_{gyr}^2 = (\sum_{i=1}^n w(i)(r(i) - \bar{r})^2) / \sum_{i=1}^n w(i)$ , where  $w(i)$  is the atomic mass,  $r(i)$  is the position of the  $i$ th atom, and  $\bar{r}$  is the center of mass of the whole protein. In the simulation, the C<sub>α</sub> atom was pulled through the water-octane interface at about  $t=33$  ns, indicated by the kinks in (B, C, D); the kinks near  $t=140$  ns, correspond to the moment the protein is fully dragged into the octane phase.

In previous work studying DNA pulling behaviours,<sup>5</sup> we noticed that counterions tended to condense around the DNA strands when DNA was pulled from water to octane. The counterions energetically compensate for the negatively charged phosphate groups on the DNA backbone. In current simulation of titin, though the protein contains only a small number of negative charges (six), it is still observed that the same number of sodium ions (six) pass through the water/oil interface with the protein.

The simulation of the second scenario suggests that during pulling, the protein will be unfolded at the water/nonpolar solvent interface. It is likely that in the single-molecule pulling experiments (the pulling speed is much lower than that in MD simulations), the required unfolding force is significantly lowered<sup>53</sup> to the noise level of AFM ( $\sim 5$  pN), such that the unfolding events can not be distinguished in the F-E curves. Other techniques with a better force resolution (for instance, optical tweezers<sup>54</sup>) will be employed to investigate whether the unfolding events indeed occur at low forces.

### 3.4 Implications for protein unfolding in vivo.

Previous as well as current experimental and MD simulation results suggest that the only precondition for DNA unwinding or protein unfolding is to pull the DNA or protein molecule from water into a nonpolar solvent environment.<sup>5</sup> It was noticed that DNA helicases could provide a relatively hydrophobic micro-environment, supporting the unwinding of DNA.<sup>5</sup> Assuming that low polarity and high hydrophobicity are equivalent in the non-liquid environment, one would expect that a hydrophobic cavity developed inside the protein facilitates unravelling the native structures of the substrate.

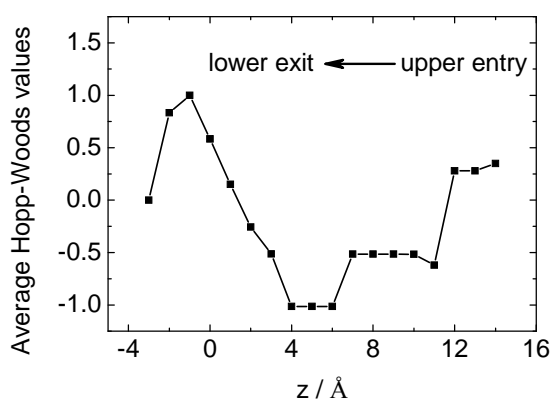


**Fig. 9.** Average hydrophilicity values (Hopp-Woods index) along the central axis inside the ClpX ring (PDB ID: 3HWS). The calculation was done for amino acids within 0.8 nm of the central axis of the ring. The protein entry is located on the right side at  $z \sim 12 \text{ \AA}$ . A low average Hopp-Woods value is indicative of a high hydrophobicity.

To further probe if a change of hydrophobicity of the environment also takes place in the protein-unfolding machines, we analyzed a protease motor protein ClpX.<sup>54-56</sup> It is a hexameric ring-shaped enzyme from *E. coli* using free energy from ATP hydrolysis to unfold native proteins and to translocate the unfolded polypeptides into the peptidase ClpP. In Fig. 9, we plotted the

average Hopp-Woods indices along the central axis of the ClpX ring, which are calculated for the surrounding amino acids (within a distance of 0.8 nm of the central axis). It is shown that the local environment inside ClpX changes to low Hopp-Woods values (high hydrophobicity) below the ClpX entry (at  $z \sim 12 \text{ \AA}$ ). Therefore, a hydrophilic/hydrophobic interface that similar to those in the MD simulations (Fig. 7) will be formed at the entry of protease. Interestingly, other proteases, such as PAN/20S (PDB ID: 3IPM) and HsIU (PDB ID: 1G3I), also show the similar trend of the hydrophobicity change (see ESI for details). Thus, the proteases seem to provide a hydrophilic/hydrophobic interface to facilitate protein unfolding and/or stabilize the unfolded structure. Therefore, it is likely that this mechanism is widely employed in protein machines, for not only DNA unwinding helicases, but also protein unfolding proteases.

## 4. Conclusions

In summary, we have observed by single-molecule AFM that the polyprotein, I27<sub>8</sub>, is unfolded completely when it is pulled from aqueous buffer to nonpolar solvent. This result is supported by force measurements of the polyprotein in a denaturant solution, a theoretical F-E curve of a polypeptide, and a direct comparison with an unstructured polypeptide, polylysine. MD simulation also indicates that a protein will unfold when it is pulled across the water/nonpolar solvent interface. Furthermore, MD simulation suggests that the nonpolar solvent alone does not induce protein unfolding, supporting our conclusion that it is the pulling process across the water/nonpolar solvent interface that leads to the protein unfolding. Further investigation reveals that cellular proteases have a low polarity cavity, which may facilitate the unfolding of the protein substrate and/or stabilize the unfolded structure. This low polarity environment effect may be utilized by a broad class of molecular machines to unfold/unwind substrates in the cavity.

## ACKNOWLEDGMENTS

We thank Carlos Bustamante for helpful discussions and careful revision of the manuscript. This work was supported by the National Basic Research Program (2011CB707604), the Natural Science Foundation of China (21222401), the program for New Century Excellent Talents in University (NCET-11-0708), and the Fundamental Research Funds for the Central Universities (SWJTU11ZT05, SWJTU12CX001).

## Notes and references

- <sup>a</sup> Key Lab of Advanced Technologies of Materials, Ministry of Education of China, Southwest Jiaotong University, Chengdu 610031, China. Email: cui shuxun@swjtu.edu.cn
- <sup>b</sup> Beijing Computational Science Research Center, Chinese Academy of Engineering Physics, Beijing 100084, China. Email: jinyu@csrc.ac.cn
- <sup>c</sup> The California Institute for Quantitative Biosciences (QB3), University of California, Berkeley, Berkeley, CA 94720, USA
- † Electronic Supplementary Information (ESI) available: the schematic diagram of environment change, the comparison of F-E curves obtained at

- various stretching velocities, the details of QM-WLCmodel and the process of the generation of a fitting curves, the comparison of F-E curves of polylysine obtained in PBS and I27<sub>s</sub> obtained in 6M GdnHCl, the normalized F-E curves of polylysine obtained in PBS solution, MD simulation movies, the hydrophobicity change of PAN/20S and HsIU. See DOI: 10.1039/b000000x/
1. A. Matouschek, *Curr. Opin. Struct. Biol.*, 2003, **13**, 98-109.
  2. R. T. Sauer and T. A. Baker, *Annu. Rev. Biochem.*, 2011, **80**, 587-612.
  3. C. Tanford, *Adv. Prot. Chem.*, 1970, **24**, 1-95.
  4. K. Tanaka and Y. Okahata, *J. Am. Chem. Soc.*, 1996, **118**, 10679-10683.
  5. S. Cui, J. Yu, F. Kuehner, K. Schulten and H. E. Gaub, *J. Am. Chem. Soc.*, 2007, **129**, 14710-14716.
  6. M. Rief, M. Gautel, F. Oesterhelt, J. M. Fernandez and H. E. Gaub, *Science*, 1997, **276**, 1109-1112.
  7. A. Janshoff, M. Neitzert, Y. Oberdorfer and H. Fuchs, *Angew. Chem. Int. Ed.*, 2000, **39**, 3212-3237.
  8. W. Zhang and X. Zhang, *Prog. Polym. Sci.*, 2003, **28**, 1271-1295.
  9. J. M. Fernandez and H. Li, *Science*, 2004, **303**, 1674-1678.
  10. S. Morris, S. Hanna and M. J. Miles, *Nanotechnology*, 2004, **15**, 1296-1301.
  11. S. Zou, H. Schonherr and G. J. Vancso, *Angew. Chem. Int. Ed.*, 2005, **44**, 956-959.
  12. M. Geisler, R. R. Netz and T. Hugel, *Angew. Chem. Int. Ed.*, 2010, **49**, 4730-4733.
  13. S. Lv, D. M. Dudek, Y. Cao, M. M. Balamurali, J. Gosline and H. Li, *Nature*, 2010, **465**, 69-73.
  14. I. T. S. Li and G. C. Walker, *Proc. Natl. Acad. Sci. USA.*, 2011, **108**, 16527-16532.
  15. K. Liu, Y. Song, W. Feng, N. Liu, W. Zhang and X. Zhang, *J. Am. Chem. Soc.*, 2011, **133**, 3226-3229.
  16. I. Popa, B. Zhang, P. Maroni, A. D. Schlueter and M. Borkovec, *Angew. Chem. Int. Ed.*, 2010, **49**, 4250-4253.
  17. F. Valle, G. Zuccheri, A. Bergia, L. Ayres, A. E. Rowan, R. J. M. Nolte and B. Samori, *Angew. Chem. Int. Ed.*, 2008, **47**, 2431-2434.
  18. P. E. Marszalek and Y. F. Dufrene, *Chem. Soc. Rev.*, 2012, **41**, 3523-3534.
  19. M. Rangl, A. Ebner, J. Yamada, C. Rankl, R. Tampe, H. J. Gruber, M. Rexach and P. Hinterdorfer, *Angew. Chem. Int. Ed.*, 2013, **52**, 10356-10359.
  20. M. Carrion-Vazquez, A. F. Oberhauser, T. E. Fisher, P. E. Marszalek, H. Li and J. M. Fernandez, *Prog. Biophys. Mol. Biol.*, 2000, **74**, 63-91.
  21. W. Zhao, M. Cai, H. Xu, J. Jiang and H. Wang, *Nanoscale*, 2013, **5**, 3226-3229.
  22. Y. Pan, F. Wang, Y. Liu, J. Jiang, Y.-G. Yang and H. Wang, *Nanoscale*, 2014, **6**, 9951-9954.
  23. Y. Bao, H.-J. Qian, Z.-Y. Lu and S. Cui, *Nanoscale*, 2014, **6**, 13421-13424.
  24. C. Lv, X. Gao, W. Li, B. Xue, M. Qin, L. D. Burtnick, H. Zhou, Y. Cao, R. C. Robinson and W. Wang, *Nat. Commun.*, 2014, **5**, 4623.
  25. J. Chung, A. M. Kushner, A. C. Weisman and Z. Guan, *Nat Mater.*, 2014, **13**, 1055-1062.
  26. A. Embrechts, H. Schonherr and G. J. Vancso, *J. Phys. Chem. B*, 2012, **116**, 565-570.
  27. V. Walhorn, C. Schafer, T. Schroder, J. Mattay and D. Anselmetti, *Nanoscale*, 2011, **3**, 4859-4865.
  28. A. Touhami, M. Alexander, M. Kurylowicz, C. Gram, M. Corredig and J. R. Dutcher, *Soft Matter*, 2011, **7**, 10274-10284.
  29. J. Stigler, F. Ziegler, A. Gieseke, J. C. Gebhardt and M. Rief, *Science*, 2011, **334**, 512-516.
  30. P. Lussis, T. Svaldo-Lanero, A. Bertocco, C. A. Fustin, D. A. Leigh and A. S. Duwez, *Nat. Nanotechnol.*, 2011, **6**, 553-557.
  31. Y. Song, W. Feng and W. Zhang, *Chinese J. Polym. Sci.*, 2014, **32**, 1149-1157.
  32. H. Lu and K. Schulten, *Biophys. J.* 2000, **79**, 51-65.
  33. H. Grubmuller, B. Heymann and P. Tavan, *Science*, 1996, **271**, 997-999.
  34. T. Hugel and M. Seitz, *Macromol. Rapid Commun.*, 2001, **22**, 989-1016.
  35. S. Cui, X. Pang, S. Zhang, Y. Yu, H. Ma and X. Zhang, *Langmuir*, 2012, **28**, 5151-5157.
  36. S. Improta, A. S. Politou and A. Pastore, *Structure*, 1996, **4**, 323-337.
  37. W. L. Jorgensen, J. Chandrasekhar, J. D. Madura, R. W. Impey and M. L. Klein, *J. Chem. Phys.*, 1983, **79**, 926-935.
  38. J. C. Phillips, R. Braun, W. Wang, J. Gumbart, E. Tajkhorshid, E. Villa, C. Chipot, R. D. Skeel, L. Kale and K. Schulten, *J. Comput. Chem.*, 2005, **26**, 1781-1802.
  39. B. R. Brooks, R. E. Bruccoleri, B. D. Olafson, D. J. States, S. Swaminathan and M. Karplus, *J. Comput. Chem.*, 1983, **4**, 187-217.
  40. P. F. Batcho, D. A. Case and T. Schlick, *J. Chem. Phys.*, 2001, **115**, 4003-4018.
  41. J. F. Marko and E. D. Siggia, *Macromolecules*, 1995, **28**, 8759-8770.
  42. W. A. Linke, M. Ivemeyer, P. Mundel, M. R. Stockmeier and B. Kolmerer, *Proc. Natl. Acad. Sci. USA.*, 1998, **95**, 8052-8057.
  43. C. Bustamante, J. F. Marko, E. D. Siggia and S. Smith, *Science (Washington, D.C.)*, 1994, **265**, 1599-1600.
  44. M. Carrion-Vazquez, A. F. Oberhauser, S. B. Fowler, P. E. Marszalek, S. E. Broedel, J. Clarke and J. M. Fernandez, *Proc. Natl. Acad. Sci. USA.*, 1999, **96**, 3694-3699.
  45. S. X. Cui, C. Albrecht, F. Kuhner and H. E. Gaub, *J. Am. Chem. Soc.*, 2006, **128**, 6636-6639.
  46. T. Hugel, M. Rief, M. Seitz, H. Gaub and R. Netz, *Phys. Rev. Lett.*, 2005, **94**, 048301.
  47. S. Cui, Y. Yu and Z. Lin, *Polymer*, 2009, **50**, 930-935.
  48. L. Tskhovrebova, J. Trinick, J. A. Sleep and R. M. Simmons, *Nature*, 1997, **387**, 308-312.
  49. D. B. Asay and S. H. Kim, *J. Phys. Chem. B*, 2005, **109**, 16760-16763.
  50. P. J. Halling, *Biochim. Biophys. Acta*, 1990, **1040**, 225-228.
  51. A. M. Klibanov, *Trends Biotechnol.*, 1997, **15**, 97-101.
  52. P. L. Privalov and S. J. Gill, *Adv. Protein. Chem.*, 1988, **39**, 191-234.
  53. F. Rico, L. Gonzalez, I. Casuso, M. Puig-Vidal and S. Scheuring, *Science*, 2013, **342**, 741-743.
  54. R. A. Maillard, G. Chistol, M. Sen, M. Righini, J. Tan, C. M. Kaiser, C. Hodges, A. Martin and C. Bustamante, *Cell*, 2011, **145**, 459-469.
  55. M. E. Aubin-Tam, A. O. Olivares, R. T. Sauer, T. A. Baker and M. J. Lang, *Cell*, 2011, **145**, 257-267.
  56. S. E. Glynn, A. Martin, A. R. Nager, T. A. Baker and R. T. Sauer, *Cell*, 2009, **139**, 744-756.